OXFORD CENTRE FOR COLLABORATIVE APPLIED MATHEMATICS

Report Number 11/37

Frequency jumps in the planar vibrations of an elastic beam

by

Sébastien Neukircha, Jöel Frelata, Alain Goriely, Corrado Maurinia

Oxford Centre for Collaborative Applied Mathematics
Mathematical Institute
24 - 29 St Giles'
Oxford
OX1 3LB
England

Frequency jumps in the planar vibrations of an elastic beam

Sébastien Neukirch[a,b], Joël Frelat[a,b], Alain Goriely[c], Corrado Maurini[a,b]

[a] *CNRS, UMR 7190, Institut Jean Le Rond d'Alembert, F-75005 Paris, France.*
[b] *UPMC Univ Paris 06, UMR 7190, Institut Jean Le Rond d'Alembert, F-75005 Paris, France.*
[c] *Oxford Centre for Collaborative Applied Mathematics (OCCAM), Oxford University, U.K.*

Abstract

The small amplitude transverse vibrations of an elastic beam clamped at both extremities are studied. The beam is modeled as an extensible, shearable planar Kirchhoff elastic rod under large displacements and rotations, and the vibration frequencies are computed both analytically and numerically as a function of the loading. Of particular interest is the variation of mode frequencies as the load is increased through the buckling threshold. While for some modes there is no qualitative changes in the mode frequencies, other modes experience rapid variations after the buckling threshold. For slender beams, these variations become stiffer, eventually resulting in a discontinuous jump of frequency at buckling, in the limit of inextensible, unshearable beams.

Keywords: Vibrations, Kirchhoff elastic rods, Buckling, Bifurcation.

1. Introduction

The first step in the study of vibrating elastic structures [1] focuses on the dynamical response of the system around its unstressed configuration. In vibration analysis, the dynamics of infinitely small amplitude disturbances around the fundamental equilibrium state are generally first considered, leading to a linear problem. However, nonlinear effects are known to play a key role in many elastic systems, and in the context of vibrations, nonlinearities can be included by studying large amplitude oscillations around the fundamental state [2]. The second step in the analysis of vibrations is to study the effect of external loads. They have a direct influence on the dynamical response of the system, as easily demonstrated by tuning the natural frequencies of a string by putting it under tension. Similarly, in compression, the natural frequencies of a beam decrease. Again nonlinear effects become important when external loads not only change the vibration response of the beam but also alter its overall stability through buckling. Strangely, relatively few studies are devoted to the dynamical response of an elastic structure around its post-buckled state. The present work focuses on the problem of small amplitude vibrations around a pre-strained deformed nonlinear elastic beam. This problem is relevant for a number of applications including the manufacturing of piano (or violin) soundboards where the wooden board is bent before being clamped in the rigid metal frame [3, 4, 5]. Other systems where pre-stress and/or pre-strain play an important role for the vibration response are gongs, cymbals, or steel drums where plastic deformations of the metal plates are used to introduce separation of response modes [6].

More precisely, we consider here the problem of vibrations of a pre- and post-buckled planar Kirchhoff extensible shearable elastic beam. First, we study the equilibrium configurations of

a clamped-clamped beam as the axial displacement is gradually increased. The beam has a straight natural shape and for small displacements the beam remains straight, until a critical axial displacement is reached where the beam buckles in the plane. For each value of the axial displacement we study the small amplitude vibrations around the equilibrium state and we follow how frequencies of the natural modes change as the load is increased. For both equilibrium and vibrations we enforce a rigid loading condition, that is, the axial displacement rather that the axial load is imposed. The paper is organised as follows: In Section 2 we present the Kirchhoff model for elastic beams, in Section 3 we derive the equations for the small amplitude vibrations of a beam around its post-buckled equilibrium, in Section 4 we solve these equations numerically for extensible as well as for inextensible beams and demonstrate the existence of jumps in frequency for inextensible beams at the critical load. In section 5 we calculate the frequency gaps in the inextensible case, and in section 6 we compare our results with a classical weakly nonlinear equation (see e.g. [1]).

2. Model

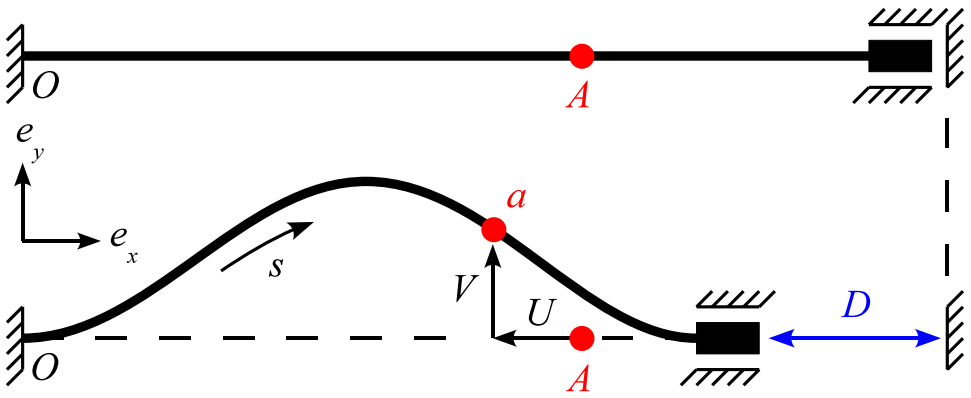

Figure 1: Clamped-Clamped beam buckled in the (x,y) plane. The end-shortening D is controlled. The point A in the reference configuration moves to point a in the deformed configuration, introducing horizontal $U \leq 0$ and vertical V displacements. The origin is taken at the fixed point O at the left end of the beam.

We consider an elastic beam with a rectangular cross-section of width b and thickness h, total length L and arc length S in its unstressed reference state. In this state the beam lies along the $\boldsymbol{e_x}$ axis, from the origin $O = (0,0,0)$ to the point at $(L,0,0)$. The position vector of the center of the beam cross-section is noted $\boldsymbol{R}(S)$ and we have $\boldsymbol{R}(S=0) = (0,0,0)$ and $\boldsymbol{R}(S=L) = (L,0,0)$ in the reference state.

Kinematics

We consider a Timoshenko beam, that is a beam that can suffer bending, extension, and shear deformations. We work under the assumption that the beam cross section remains planar (and rectangular) as the beam deforms and use a set of three Cosserat directors $(\boldsymbol{d_1}(S), \boldsymbol{d_2}(S), \boldsymbol{d_3}(S))$ embedded in each cross-section: $\boldsymbol{d_1}$ is perpendicular to the section plane, $\boldsymbol{d_2}$ is along the small span (of length h) of the section, and $\boldsymbol{d_3}$ is along the wide span (of length b) of the section. In

the undeformed state, $\boldsymbol{d_1}(S) \equiv \boldsymbol{e_x}$, $\boldsymbol{d_2}(S) \equiv \boldsymbol{e_y}$, and $\boldsymbol{d_3}(S) \equiv \boldsymbol{e_z}$, $\forall\, S$. We only consider deformed states that are (*i*) planar (where the beam center line $\boldsymbol{R}(S)$ lies in the (x, y) plane), and (*ii*) twistless (where the director $\boldsymbol{d_3}(S) \equiv \boldsymbol{e_z}$, $\forall\, S$). Note that in the presence of extension and shear, S may no longer be the arc-length of the curve $\boldsymbol{R}(S)$ in the deformed state. We introduce extension and shear strains, e_1 and e_2, such that:

$$\boldsymbol{R}'(S) \stackrel{\text{def}}{=} \mathrm{d}\boldsymbol{R}/\mathrm{d}s = (1 + e_1)\,\boldsymbol{d_1} + e_2\,\boldsymbol{d_2}\,. \tag{1}$$

In the absence of extension ($e_1 = 0$) and shear ($e_2 = 0$), the director $\boldsymbol{d_1}$ is the tangent to the centerline $\boldsymbol{R}(S) = (X(S), Y(S), Z(S))$. We introduce the angle $\theta(S)$ to parametrize the rotation of the $(\boldsymbol{d_1}, \boldsymbol{d_2})$ frame around the $\boldsymbol{e_z} = \boldsymbol{d_3}$ axis:

$$\boldsymbol{d_1}(S) = \left.\begin{pmatrix} \cos\theta(S) \\ \sin\theta(S) \\ 0 \end{pmatrix}\right|_{\boldsymbol{e_x},\boldsymbol{e_y},\boldsymbol{e_z}} \quad \text{and} \quad \boldsymbol{d_2}(S) = \left.\begin{pmatrix} -\sin\theta(S) \\ \cos\theta(S) \\ 0 \end{pmatrix}\right|_{\boldsymbol{e_x},\boldsymbol{e_y},\boldsymbol{e_z}}. \tag{2}$$

Dynamics

We use the Kirchhoff dynamical equations for elastic rods [7], where the stresses in the section are averaged to yield an internal force $\boldsymbol{N}(S)$ and an internal moment $\boldsymbol{M}(S)$. These internal forces and moments are the loads exerted on the section at S by the part of the beam at $\bar{S} > S$. The linear and angular momentum dynamical equations then read

$$\boldsymbol{N}'(S,T) = \rho\, h\, b\, \ddot{\boldsymbol{R}}(S,T), \tag{3}$$

$$\boldsymbol{M}'(S,T) + \boldsymbol{R}'(S,T) \times \boldsymbol{N}(S,T) = \rho\, I\, \ddot{\theta}(S,T)\,, \tag{4}$$

where $\dot{(\,)} \stackrel{\text{def}}{=} \mathrm{d}/\mathrm{d}T$, T is time, ρ the mass per unit volume of the material, and I the second moment of area of the cross-section (in the present case $I = h^3 b/12$).

Constitutive law

We use the standard linear constitutive relationship relating the bending strain $\kappa(S) \stackrel{\text{def}}{=} \theta'(S)$ to the bending moment $M_3 \stackrel{\text{def}}{=} \boldsymbol{M} \cdot \boldsymbol{d_3}$:

$$M_3 = E\, I\, \kappa, \tag{5}$$

where E is the Young's modulus. In a similar way, the tension $N_1 \stackrel{\text{def}}{=} \boldsymbol{N} \cdot \boldsymbol{d_1}$ and the shear force $N_2 \stackrel{\text{def}}{=} \boldsymbol{N} \cdot \boldsymbol{d_2}$ are linked to the extension e_1 and shear strains e_2 through

$$N_1 = E\, h\, b\, e_1, \tag{6}$$

$$N_2 = G\, h\, b\, e_2. \tag{7}$$

where G is the shear modulus.

Equations in component form

In the planar case considered here, we have $Z(S,T) \equiv 0$, $N_z(S,T) \equiv 0$, $M_x(S,T) \equiv 0$, and $M_y(S,T) \equiv 0$, $\forall (S,T)$ so that the equations for the six remaining unknowns are

$$\begin{aligned} X' &= (1+e_1)\cos\theta - e_2 \sin\theta, && \text{(8a)}\\ Y' &= (1+e_1)\sin\theta + e_2 \cos\theta, && \text{(8b)}\\ \theta' &= M/(EI), && \text{(8c)}\\ M' &= e_2\, N_1 - (1+e_1)\, N_2 + \rho I \ddot{\theta}, && \text{(8d)}\\ N_x' &= \rho h b\, \ddot{X}, && \text{(8e)}\\ N_y' &= \rho h b\, \ddot{Y}, && \text{(8f)} \end{aligned}$$

where $M = M_z = M_3$, $N_1 = N_x \cos\theta + N_y \sin\theta$, and $N_2 = -N_x \sin\theta + N_y \cos\theta$. The strains (e_1, e_2) are then given by Eqs (6) and (7).

Dimensionless variables

We scale all lengths with L, time with $\tau \overset{\text{def}}{=} L^2 \sqrt{\rho h b/(EI)}$, forces with EI/L^2, and moments with EI/L. This naturally introduces a parameter

$$\eta \overset{\text{def}}{=} \frac{I}{hbL^2} = \frac{1}{12}\left(\frac{h}{L}\right)^2, \qquad (9)$$

which takes small values in the present case of slender beams. Dimensionless variables will be written lowercase, e.g. $x \overset{\text{def}}{=} X/L$, or $m \overset{\text{def}}{=} ML/(EI)$. The constitutive relations (6) and (7) reads: $e_1 = \eta\, n_1$ and $e_2 = 2(1+\nu)\,\eta\, n_2$, where the Poisson ratio ν arises from the relation $E = 2(1+\nu)\,G$.

Beams with $\eta > 0$ will be called *Timoshenko* beams and beams with $\eta = 0$ will be called *elasticas*. An elastica is therefore an inextensible, unshearable beam for which the rotational inertia has been ignored.

3. Small amplitude vibrations around post-buckled equilibrium

The systems of equations (8) in dimensionless form reads

$$\begin{aligned} x'(s,t) &= \cos\theta + \eta\,(n_1\, \cos\theta - 2(1+\nu)\, n_2 \sin\theta)\,, && \text{(10a)}\\ y'(s,t) &= \sin\theta + \eta\,(n_1\, \sin\theta + 2(1+\nu)\, n_2 \cos\theta)\,, && \text{(10b)}\\ \theta'(s,t) &= m, && \text{(10c)}\\ m'(s,t) &= -n_2 + \eta\left((1+2\nu)\, n_1\, n_2 + \ddot{\theta}\right), && \text{(10d)}\\ n_x'(s,t) &= \ddot{x}, && \text{(10e)}\\ n_y'(s,t) &= \ddot{y}, && \text{(10f)} \end{aligned}$$

with $n_1 = n_x \cos\theta + n_y \sin\theta$ and $n_2 = -n_x \sin\theta + n_y \cos\theta$. In our problem, we consider a clamped-clamped beam and control the end-shortening $d \overset{\text{def}}{=} 1 - (x(1,t) - x(0,t))$. This setup implies the following boundary conditions

$$\begin{aligned} x(0,t) = 0 \qquad & x(1,t) = 1 - d\,, && \text{(11a)}\\ y(0,t) = 0 \qquad & y(1,t) = 0\,, && \text{(11b)}\\ \theta(0,t) = 0 \qquad & \theta(1,t) = 0\,. && \text{(11c)} \end{aligned}$$

For each given value of the end-shortening d, we find the equilibrium configuration $(x_e, y_e, \theta_e, m_e, n_{xe}, n_{ye})$ by solving system (10) with $\ddot{x}_e = 0$ and $\ddot{y}_e = 0$. Then we look for small amplitude vibrations around this equilibrium configuration, that is, we set

$$
\begin{aligned}
x(s,t) &= x_e(s) + \delta\, \bar{x}(s)\, \mathrm{e}^{\mathrm{i}\omega t}, && \text{(12a)}\\
y(s,t) &= y_e(s) + \delta\, \bar{y}(s)\, \mathrm{e}^{\mathrm{i}\omega t}, && \text{(12b)}\\
\theta(s,t) &= \theta_e(s) + \delta\, \bar{\theta}(s)\, \mathrm{e}^{\mathrm{i}\omega t}, && \text{(12c)}\\
m(s,t) &= m_e(s) + \delta\, \bar{m}(s)\, \mathrm{e}^{\mathrm{i}\omega t}, && \text{(12d)}\\
n_x(s,t) &= n_{xe}(s) + \delta\, \bar{n}_x(s)\, \mathrm{e}^{\mathrm{i}\omega t}, && \text{(12e)}\\
n_y(s,t) &= n_{ye}(s) + \delta\, \bar{n}_y(s)\, \mathrm{e}^{\mathrm{i}\omega t}, && \text{(12f)}
\end{aligned}
$$

where $\delta \ll 1$ is a small parameter. Inserting (12) into (10) and keeping only linear terms in δ, we obtain equations for the spatial modes $(\bar{x}, \bar{y}, \bar{\theta}, \bar{m}, \bar{n}_x, \bar{n}_y)$:

$$
\begin{aligned}
\bar{x}'(s) &= -\bar{\theta}\, \sin\theta_e + \eta\,(\bar{n}_1\, \cos\theta_e - 2(1+\nu)\,\bar{n}_2 \sin\theta_e) + \\
&\quad \eta\,\bar{\theta}\,(-n_{1e}\, \sin\theta_e - 2(1+\nu)\, n_{2e} \cos\theta_e)\,, && \text{(13a)}\\
\bar{y}'(s) &= \bar{\theta}\, \cos\theta_e + \eta\,(\bar{n}_1\, \sin\theta_e + 2(1+\nu)\,\bar{n}_2 \cos\theta_e) + \\
&\quad \eta\,\bar{\theta}\,(n_{1e}\, \cos\theta_e - 2(1+\nu)\, n_{2e} \sin\theta_e)\,, && \text{(13b)}\\
\bar{\theta}'(s) &= \bar{m}, && \text{(13c)}\\
\bar{m}'(s) &= -\bar{n}_2 + \eta\left((1+2\nu)(\bar{n}_1\, n_{2e} + n_{1e}\,\bar{n}_2) - \omega^2\bar{\theta}\right), && \text{(13d)}\\
\bar{n}_x'(s) &= -\omega^2\bar{x}, && \text{(13e)}\\
\bar{n}_y'(s) &= -\omega^2\bar{y}, && \text{(13f)}
\end{aligned}
$$

with $\bar{n}_1 = \bar{n}_x \cos\theta_e + \bar{n}_y \sin\theta_e + \bar{\theta}\left(-n_{xe}\sin\theta_e + n_{ye}\cos\theta_e\right)$ and $\bar{n}_2 = -\bar{n}_x \sin\theta_e + \bar{n}_y \cos\theta_e + \bar{\theta}\left(-n_{xe}\cos\theta_e - n_{ye}\sin\theta_e\right)$. The boundary conditions on the spatial modes are

$$
\begin{aligned}
&\bar{x}(0) = 0 \qquad \bar{x}(1) = 0\,, && \text{(14a)}\\
&\bar{y}(0) = 0 \qquad \bar{y}(1) = 0\,, && \text{(14b)}\\
&\bar{\theta}(0) = 0 \qquad \bar{\theta}(1) = 0\,. && \text{(14c)}
\end{aligned}
$$

For given parameters η and ν and given end-shortening d, the equilibrium $(x_e, y_e, \theta_e, m_e, n_{xe}, n_{ye})$ is first computed from (10) with $\ddot{x}_e = 0$ and $\ddot{y}_e = 0$. Then the 6D system (13) with the six boundary conditions (14) is a well-defined boundary value problem, but with the additional unknown ω. For computation purpose, we normalize the linear solution of this problem by imposing the condition

$$
\bar{m}^2(0) + \bar{n}_x^2(0) + \bar{n}_y^2(0) = 1. \qquad \text{(15)}
$$

4. Numerics

We use a 'home-made' predictor-corrector path following code to address the problem numerically. For each value of $p \overset{\text{def}}{=} -n_{xe} = -N_{xe}L^2/(EI)$ in the interval $(0; 8\pi^2)$, we first compute the equilibrium solution $(x_e, y_e, \theta_e, m_e, n_{xe}, n_{ye})$. We then solve the boundary value problem (13)-(14) numerically with a shooting method: (*i*) we first use a guess for the unknown parameters

$\chi = (\bar{m}(0), \bar{n}_x(0), \bar{n}_y(0), \omega)$ and we integrate the system (13) up to $s = 1$; (*ii*) we then check if the boundary conditions (14)-(15) are satisfied. If not, we change the guess χ accordingly (using a Newton-Raphson scheme) until the boundary conditions at $s = 1$ are satisfied. Once a solution χ_i is found for a given $p = p_i$, we set $p = p_{i+1}$ and use the value χ_i as starting guess (predictor step) for the shooting method at $p = p_{i+1}$ (corrector step). In this setup, each curve $\omega = \omega(p)$ represents a path in the numerical bifurcation diagram, and we have numerically computed the four first paths (i.e. lowest four curves $\omega = \omega(p)$) for several values of the parameter $\eta = I/(hwL^2)$.

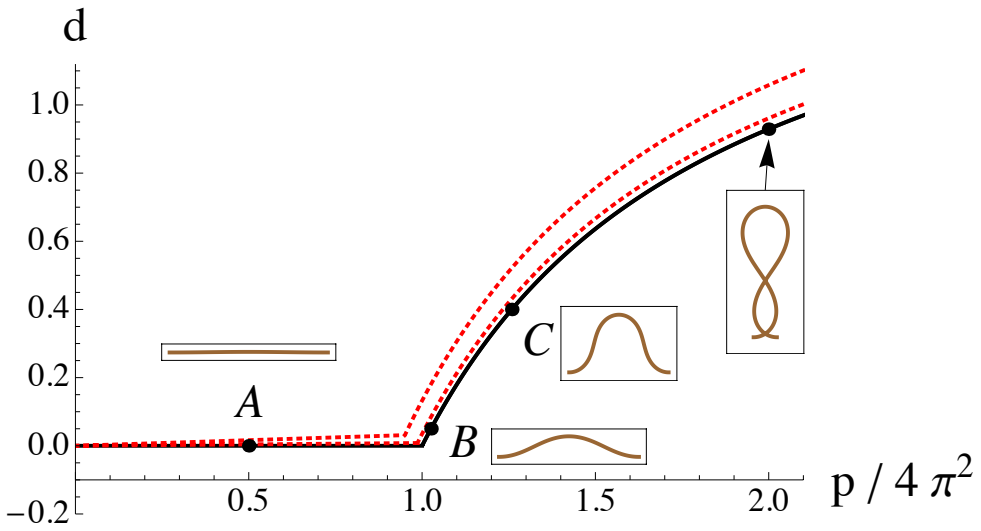

Figure 2: Fundamental and post-buckled equilibrium path of a clamped-clamped beam with $\eta = 1/1200$, $\eta = 1/4800$, and $\eta = 0$ (top to bottom). As the controlled end-shortening $d = D/L$ is gradually raised, an increasing axial load $p = -N_{xe}L^2/(EI)$ is applied.

In Fig. 2 equilibrium paths are given for both the elastica (i.e. $\eta = 0$) and the Timoshenko beam ($\eta > 0$). Buckling happens at $p = 4\pi^2$ for the elastica and at lower values for the Timoshenko beam. These equilibrium paths seem to indicate that extension and shear play a minor role in the buckling load and that the elastica solution is obtained in the limit $\eta \to 0$ of the Timoshenko solution, as expected.

In Fig. 3, pulsations for the first four modes are given as a function of the parameter p, for different values of η. It should be noted that the computations performed here are for a rigid loading experiment, where d (not p) is controlled: for each value of the applied longitudinal displacement d, the equilibrium axial load p is read from Fig. 2 and then the pulsation is computed and plotted in Fig. 3. We see in Fig. 3 that as $\eta \to 0$, pulsations globally increase and tend toward limiting curves. The limiting curves are given by the elastica case Fig. 3-(d) (also shown dashed in Fig. 3-(c)). Finally we note that for $\eta > 0$ every curve $\omega(p)$ is continuous, but that the curves for the odd modes experience a rapid increase just after buckling. As $\eta \to 0$ this rapid increase becomes stiffer to eventually turn into a finite jump in the case $\eta = 0$. This discontinuity in frequency is rather surprising and does not seem to have been reported in the literature.

In each of the Fig. 4, 5, 6, 7, 8, dynamical shapes $(x(s,t) = x_e(s) + \bar{x}(s)\cos\omega t,\ y(s,t) = y_e(s) + \bar{y}(s)\cos\omega t)$ of the vibrating beam are plotted. A tentative classification for the modes is given by the number of nodes present in $0 < s < 1$, a mode i having $i - 1$ nodes and i antinodes.

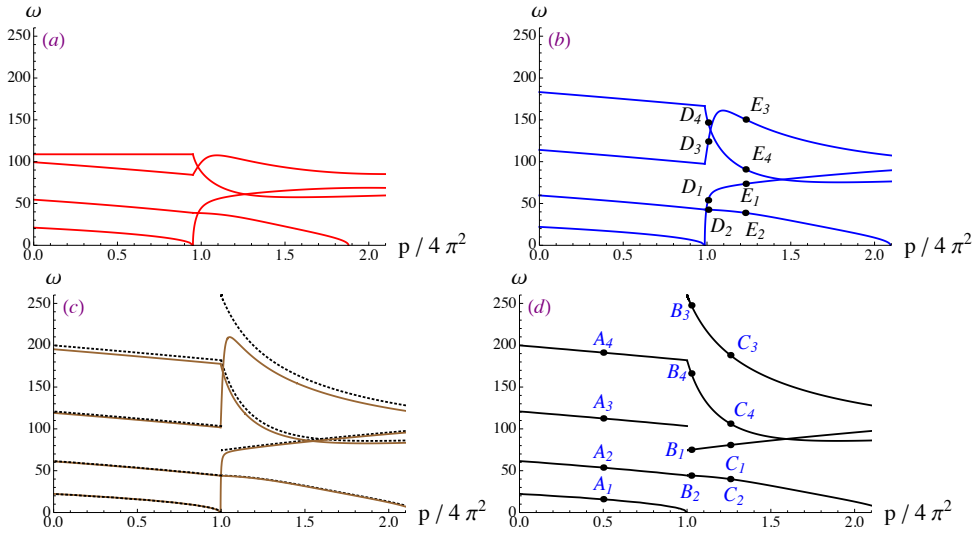

Figure 3: Pulsations for the vibration of a clamped-clamped beam around its fundamental and post-buckled equilibrium configurations: (a) for $\eta = 1/1200$, (b) for $\eta = 1/4800$, (c) for $\eta = 1/19200$ (plain) and $\eta = 0$ (dashed), and (d) for $\eta = 0$. The label A_i, B_i, C_i, D_i, and E_i with $i = 1, 2, 3, 4$ correspond to the shapes given in Fig. 4, 5, 6, 7, 8.

We see that this classification works for the modes in the pre-buckling regime (Fig. 4), but fails for the third mode in the elastica ($\eta = 0$) case (see shape B_3 in Fig. 5 and C_3 in Fig. 6) as well as in the Timoshenko ($\eta > 0$) case, provided we are far enough in the post-buckling regime (see shape E_3 in Fig. 8).

5. Analytical study

In order to understand the discontinuity of the odd modes frequencies at buckling, we look at the problem analytically. We consider an elastica, that is an inextensible, unshearable beam with no rotational inertia. Hence we set $\eta = 0$ in Eqs. (10), and we compare the frequency values just before buckling (i.e. around straight equilibrium configurations) with frequency values just after buckling (i.e. around post-buckled configurations).

Vibrations around the straight state

We first consider the equilibrium solution where the axially loaded beam is straight:

$$y_e(s) = 0,\ x_e(s) = s,\ n_{ye}(s) = 0,\ n_{xe}(s) = -p,\ \theta_e(s) = 0,\ m_e(s) = 0. \tag{16}$$

The vibrations around this straight equilibrium are $\bar{x}(s) = 0$, $\bar{n}_x(s)$ constant, and $\bar{y}(s)$ solution of:

$$\bar{y}'''' + p\,\bar{y}'' - \omega^2\,\bar{y} = 0,\ \text{with } \bar{y}(0) = 0 = \bar{y}(1),\ \text{and } \bar{y}'(0) = 0 = \bar{y}'(1)\,. \tag{17}$$

The general solution reads

$$\bar{y}(s) = A\left(\frac{\cos k^+ s - \cosh k^- s}{\cos k^+ - \cosh k^-} - \frac{k^- \sin k^+ s - k^+ \sinh k^- s}{k^- \sin k^+ - k^+ \sinh k^-}\right), \tag{18}$$

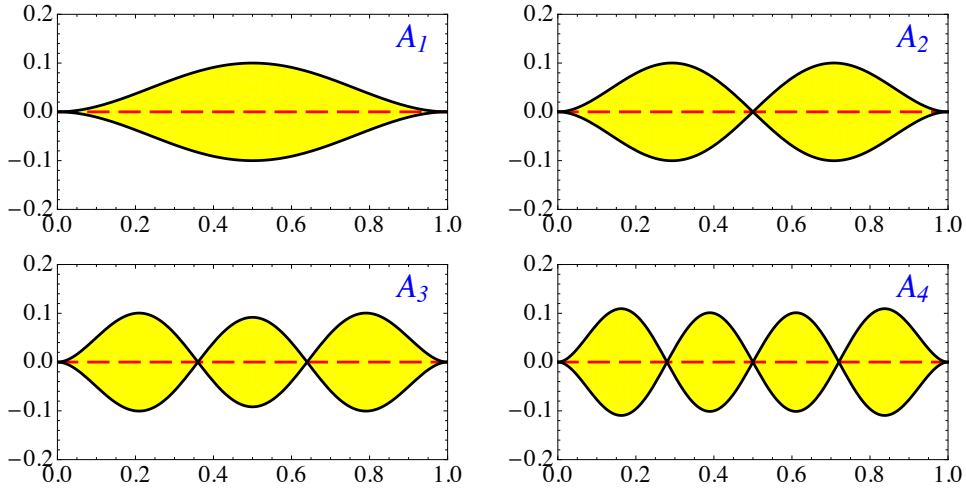

Figure 4: First four modes at $p/(4\,\pi^2) = 0.5$, in the inextensional case

with the two wave numbers $k^{\pm} = (1/\sqrt{2})\,\sqrt{\sqrt{p^2+4\omega^2} \pm p}$. The boundary conditions (17) require that either $A = 0$ or

$$2\,k^+k^-\,(\cos k^+\,\cosh k^- - 1) + p\,\sin k^+\,\sinh k^- = 0\,, \tag{19}$$

which is an equation for ω. Buckling occurs when $\omega = 0$, i.e. for $k^+ = \sqrt{p}$ and $k^- = 0$. Equation (19) then implies $k^+ = 2\pi$, hence $p = 4\pi^2$. For this critical value $p = 4\pi^2$, pulsations and wave numbers for the lowest height modes are given in Table 1. The analytical solutions $\omega(p)$ given by (19) match numerical solutions given in Fig. 3-(d).

i	1	2	3	4	5	6	7	8
ω	0	44.36	103.5	182.1	280.6	398.8	536.8	694.6
k^+	2π	8.26	11.18	14.25	17.35	20.5	23.6	26.7
$(k^+ \bmod 2\pi)/(\pi/2)$		1.26	3.12	1.07	3.04	1.03	3.02	1.02
k^-	0	5.37	9.25	12.8	16.2	19.5	22.7	25.98

Table 1: Pulsations and wave numbers for the lowest height modes of vibration around the straight state at the buckling threshold $p = 4\pi^2$, as given by Eq. (19). This also corresponds to the first height solutions of $P_1(\omega_0) = 0$ (see Eq. (29)).

Incipient post-bukled equilibrium

In the post-buckled configuration, the equilibrium equations and the boundary conditions are given by

$$n_{ye} = cte \tag{20a}$$

$$n_{xe} = -p \tag{20b}$$

$$\theta_e'' = -p\,\sin\theta_e - n_{ye}\,\cos\theta_e \;\text{ with }\; \theta_e(0) = 0 = \theta_e(1) \tag{20c}$$

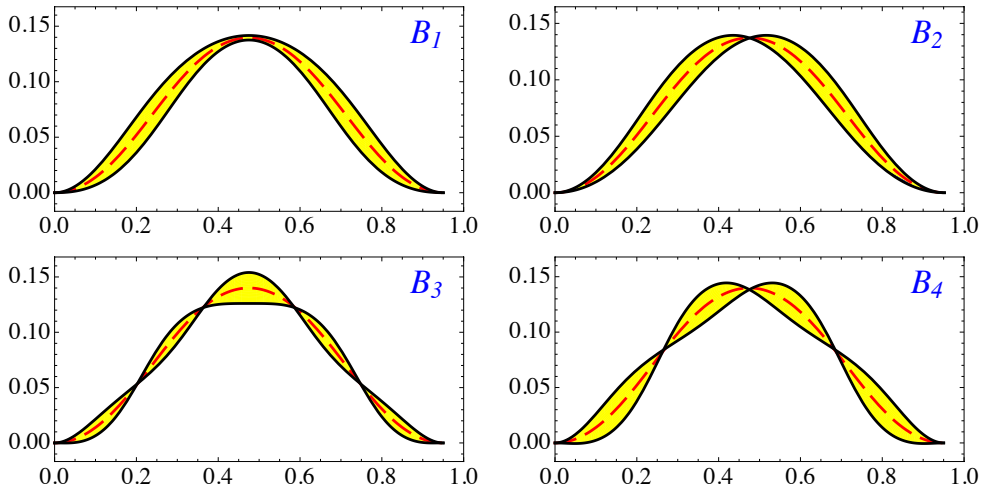

Figure 5: First four modes at $d = 0.05$, in the inextensional case

$$x_e' = \cos\theta_e \quad \text{with} \quad x_e(1) - x_e(0) = 1 - d \tag{20d}$$
$$y_e' = \sin\theta_e \quad \text{with} \quad y_e(0) = y_e(1), \tag{20e}$$

and without loss of generality, we choose $x_e(0) = y_e(0) = 0$. For equilibrium modes whose shapes are invariant when reflected along the line parallel to the $\boldsymbol{e_y}$ axis and containing the point $(x(1/2), 0)$, we have $cte = 0$ in Eq. (20a). The first bifurcated equilibrium mode, represented in Fig. 1 and on which we focus, is such a mode. We address the behavior of the solutions after but close to buckling. Therefore, we expend the variables $\theta_e(s)$ and $y_e(s)$ in powers of ϵ, a small parameter measuring the distance from buckling:

$$\theta_e(s) = \epsilon\theta_1(s) + \epsilon^2\theta_2(s) + \epsilon^3\theta_3(s) + O\left(\epsilon^4\right) \tag{21a}$$
$$x_e(s) = \epsilon x_1(s) + \epsilon^2 x_2(s) + \epsilon^3 x_3(s) + O\left(\epsilon^4\right) \tag{21b}$$
$$y_e(s) = \epsilon y_1(s) + \epsilon^2 y_2(s) + \epsilon^3 y_3(s) + O\left(\epsilon^4\right) \tag{21c}$$
$$p = p_0 + \epsilon p_1 + \epsilon^2 p_2 + \epsilon^3 p_3 + O\left(\epsilon^4\right) \tag{21d}$$

We substitute these expansions in the equilibrium equations (20), which have to be satisfied to all orders in ϵ. The solution up to order 3 reads:

$$\theta_e(s) = \epsilon \sin 2\pi s + \frac{\epsilon^3}{48}\cos^2(2\pi s)\sin(2\pi s) + O\left(\epsilon^4\right) \tag{22a}$$
$$x_e(s) = s + \frac{\epsilon^2}{16\pi}(\sin 4\pi s - 4\pi s) + O\left(\epsilon^4\right) \tag{22b}$$
$$y_e(s) = \frac{\epsilon}{2\pi}(1 - \cos 2\pi s) + \frac{\epsilon^3}{384\pi}\left(-20 + 23\cos(2\pi s) - 3\cos(6\pi s)\right) + O\left(\epsilon^4\right) \tag{22c}$$
$$p = 4\pi^2 + \epsilon^2\pi^2/2 + O\left(\epsilon^4\right) \tag{22d}$$

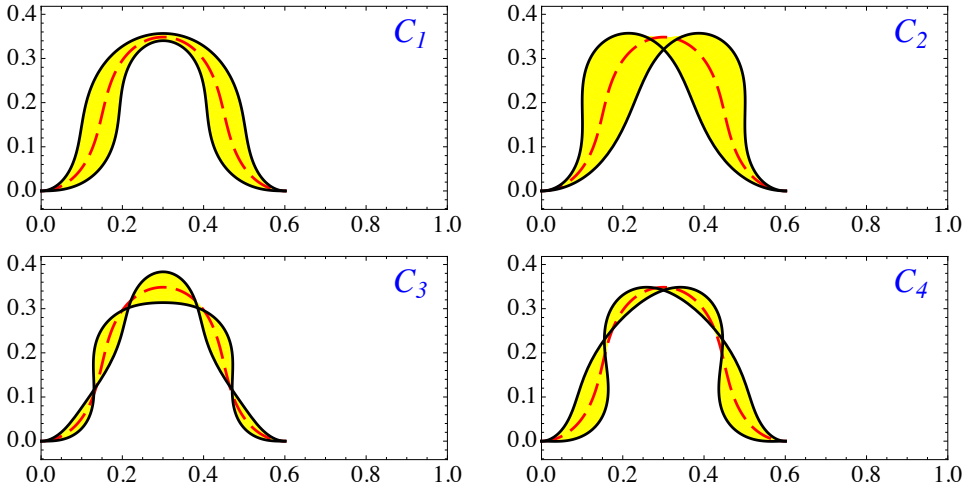

Figure 6: First four modes at $d = 0.4$, in the inextensional case

In order to relate ϵ to the control parameter d and the amplitude after bifurcation, we compute the end-shortening

$$d = 1 - (x_e(1) - x_e(0)) = \epsilon^2/4 + O\left(\epsilon^4\right) = 2\left(\frac{p}{4\pi^2} - 1\right) + O\left(\epsilon^4\right), \tag{23}$$

and the beam maximum deflection

$$y_e(1/2) = \frac{\epsilon}{\pi}\left(1 - \frac{5}{48}\,\epsilon^2\right) + O\left(\epsilon^4\right). \tag{24}$$

Vibration around the post-bukled equilibrium

We expand all modal variables $(\bar{x}, \bar{y}, \bar{\theta}, \bar{m}, \bar{n}_x, \bar{n}_y)$ and the pulsation ω in powers of ϵ. For instance, we have $\omega = \omega_0 + \epsilon\omega_1 + \epsilon^2\omega_2 + \epsilon^3\omega_3 + O\left(\epsilon^4\right)$, and so on. We can now solve equations (13) (with $\eta = 0$) with boundary conditions (14), using the equilibrium solution (22). To order ϵ^0 we have:

$$\bar{x}_0' = 0 \text{ with } \bar{x}_0(0) = 0 = \bar{x}_0(1) \tag{25a}$$

$$\bar{n}_{x0}' = -\omega_0^2\,\bar{x}_0 \tag{25b}$$

$$\bar{y}_0'''' + 4\pi^2\bar{y}_0'' - \omega_0^2\bar{y}_0 = 0 \text{ with } \bar{y}_0(0) = \bar{y}_0(1) = \bar{y}_0'(0) = \bar{y}_0'(1) = 0 \tag{25c}$$

The first two equations describe the longitudinal mode and are decoupled from the third one which is associated with the transverse mode. More precisely, the longitudinal mode is given by

$$\bar{x}_0(s) = 0 \text{ and } \bar{n}_{x0}(s) \text{ constant}. \tag{26}$$

Whereas for the transverse mode, the solution $\bar{y}_0(s)$ is

$$\bar{y}_0(s) = A_0\left(\frac{\cos k_0^+ s - \cosh k_0^- s}{\cos k_0^+ - \cosh k_0^-} - \frac{k_0^- \sin k_0^+ s - k_0^+ \sinh k_0^- s}{k_0^- \sin k_0^+ - k_0^+ \sinh k_0^-}\right), \tag{27}$$

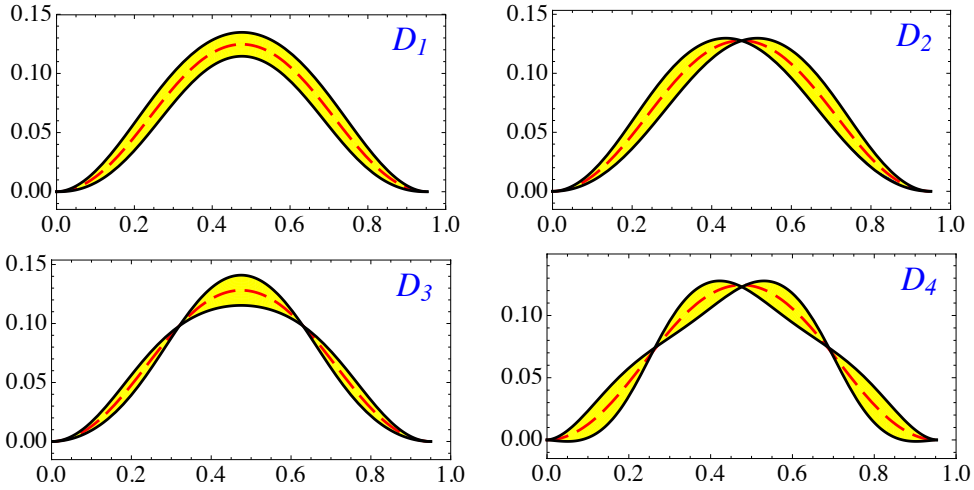

Figure 7: First four modes at $d = 0.05$, for $\eta = 1/4800$.

with $k_0^{\pm} \overset{\text{def}}{=} \sqrt{\sqrt{4\pi^4 + \omega_0^2} \pm 2\pi^2}$. The boundary conditions impose that

$$A_0\, P_1(\omega_0) = 0 \text{ with} \tag{28}$$

$$P_1(\omega_0) \overset{\text{def}}{=} 2\, k_0^+ k_0^- \left(\cos k_0^+ \cosh k_0^- - 1\right) + 4\pi^2 \sin k_0^+ \sinh k_0^- \tag{29}$$

which is an equation for ω_0. The first height solutions are listed in Table 1. Note that to order ϵ^0 there is no frequency jump. To order ϵ^1 we have

$$\bar{x}_1' = \bar{\theta}_0 \sin 2\pi s \text{ with } \bar{x}_1(0) = 0 = \bar{x}_1(1) \tag{30a}$$

$$\bar{n}_{x1}' = -\omega_0^2\, \bar{x}_1 - 2\,\omega_0\,\omega_1 \bar{x}_0 \tag{30b}$$

$$\bar{y}_1'''' + 4\pi^2 \bar{y}_1'' - \omega_0^2 \bar{y}_1 = 2\,\omega_0\,\omega_1\,\bar{y}_0 + 2\pi\,\bar{n}_{x0} \cos 2\pi s \tag{30c}$$

$$\text{with } \bar{y}_1(0) = \bar{y}_1(1) = \bar{y}_1'(0) = \bar{y}_1'(1) = 0\,. \tag{30d}$$

We start by solving equation (30a). The boundary condition $\bar{x}_1(1) = 0$ implies

$$A_0 P_2(\omega_0) = 0 \text{ with} \tag{31}$$

$$P_2(\omega_0) \overset{\text{def}}{=} k_0^+ k_0^- \left((k_0^{+2} - 2\pi^2)(\cos k_0^+ - \cosh k_0^-) + 2\pi^2(\cos k_0^+ \cosh k_0^- - 1)\right) + (k_0^{+2} k_0^{-2} + 8\pi^4) \sin k_0^+ \sinh k_0^-\,. \tag{32}$$

The solutions have to satisfy Eqs. (28) and (31), which are transcendental equations for ω_0. A numerical root finding analysis reveals that $P_1(\omega_0) = 0$ and $P_2(\omega_0) = 0$ share half of their roots, see Table 2 where columns with an even index correspond to common roots and match numerical values at $p = 4\pi^2$ for the continuous curves plotted in Fig. 3-(d). In the case of a common root, Eqs. (28) and (31) are fulfilled for non vanishing A_0, and the corresponding modes have frequencies that are continuous in the control parameter close to buckling.

In the case of distinct roots, we are compelled to set $A_0 = 0$. In this case where $P_1(\omega_0) \neq 0$, we solve Eqs. (30a) and (30b) to obtain $\bar{x}_1(s) = 0$ and $\bar{n}_{x1}(s)$ constant. The general solution of

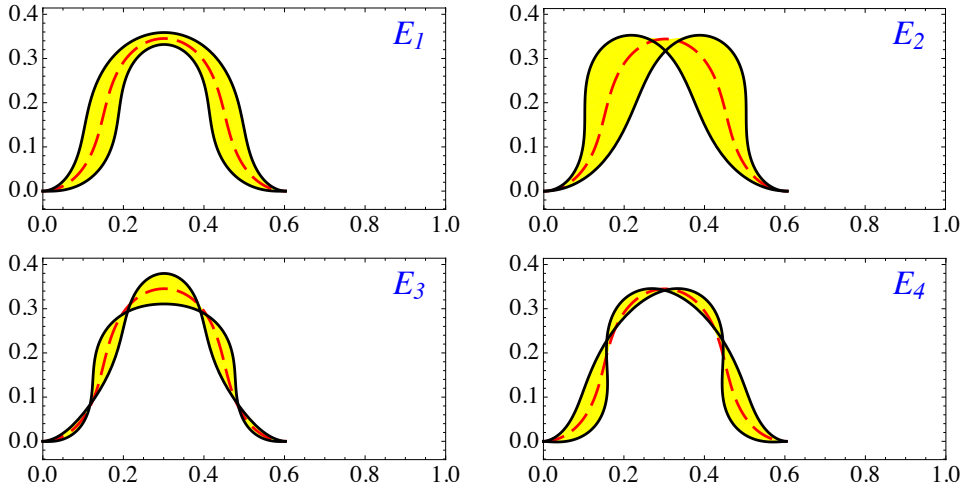

Figure 8: First four modes at $d = 0.4$, for $\eta = 1/4800$.

i	1	2	3	4	5	6	7	8
ω_0	0	44.36	169.4	182.1	390.6	398.8	688.5	694.6
k_0^+	2π	8.26	13.8	14.25	20.3	20.5	26.6	26.7
$(k_0^+ \bmod 2\pi)/(\pi/2)$		1.26	0.78	1.07	0.90	1.03	0.95	1.02
k_0^-	0	5.37	12.3	12.8	19.3	19.5	25.8	25.98

Table 2: First height solutions of $P_2(\omega_0) = 0$ (see Eq. (32)).

184 Eqs. (30c), (30d) is then

$$\begin{aligned}\bar{y}_1(s) &= \frac{2\pi\,\bar{n}_{x0}}{k_0^{+2}\,k_0^{-2}\,P_1(\omega_0)}\Big[c_1 k_0^+\cos k_0^+ s - c_1 k_0^+\cosh k_0^- s - c_2 k_0^-\sin k_0^+ s + c_2 k_0^+\sinh k_0^- s \\ &\quad + P_1(\omega_0)(\cos k_0^+ s - \cos 2\pi s)\Big] \qquad (33)\end{aligned}$$

185 where

$$c_1 = k_0^-(\cos k_0^+ - 1)(\cosh k_0^- + 1) + k_0^+\sin k_0^+\,\sinh k_0^- \qquad (34)$$

$$c_2 = k_0^+\sin k_0^+(\cosh k_0^- - 1) + k_0^-(\cos k_0^+ - 1)\sinh k_0^- \qquad (35)$$

186 In order to select a mode, we need to proceed to order ϵ^2, which reads

$$\bar{x}_2'(s) = -\bar{y}_1'(s)\ \sin 2\pi s \text{ with } \bar{x}_2(0) = 0 = \bar{x}_2(1) \qquad (36)$$

187 The boundary conditions at $s = 1$ imposes $P_3(\omega_0)/P_1(\omega_0) = 0$ where

$$\begin{aligned}P_3(\omega_0) &= 2k_0^{-2}k_0^{+2}(\cosh k_0^-\cos k_0^+ - 1) - 4k_0^+(k_0^{-2} + k_0^{+2})\sin k_0^+(\cosh k_0^- - 1) \\ &\quad + (4k_0^-(k_0^{-2} + k_0^{+2})(1 - \cos k_0^+) + 4\pi^2 k_0^- k_0^+\sin k_0^+)\sinh k_0^- \qquad (37)\end{aligned}$$

Oddly enough this function $P_3(\omega_0)$ has the same set of common roots as $P_1(\omega_0)$ and $P_2(\omega_0)$, see Table 3. The other roots correspond to the pulsation values at which the (discontinuous) odd mode curves emerge from $p = 4\pi^2$ in Fig. 3-(d). Moreover one can verify that

$$P_3(\omega_0) = k_0^+ k_0^- P_1(\omega_0) - 8\left(k_0^{+2} + k_0^{-2}\right)\left(k_0^+ \cos\frac{k_0^+}{2}\tanh\frac{k_0^-}{2} - k_0^- \sin\frac{k_0^+}{2}\right)\sinh k_0^- \sin\frac{k_0^+}{2} \tag{38}$$

which implies that the common roots must verify:

$$\frac{k_0^+}{2}\tanh\frac{k_0^-}{2} = \frac{k_0^-}{2}\tan\frac{k_0^+}{2} \tag{39}$$

These roots correspond to frequencies that do not vary abruptly after buckling has occurred. An approximate formula is $k_0^+ \simeq \pi/2 + 2j\pi$ (with positive integers j), which yields $\omega_0 \simeq (\pi/2)^2(4j+1)\sqrt{(4j-3)(4j+5)}$ (corresponding to columns with $i > 1$ even in Table 3).

Formulas for the roots of the three functions P_1, P_2, and P_3 in the limit of large k_0^+ are given in Appendix C. In particular it is shown that the set of roots of P_3 which is not in common with P_1 and P_2 is such that $k_0^+ \simeq 3\pi/2 + 2j\pi$ (with positive integers j). This implies that the frequencies emerging from buckling are such that $\omega_0 \simeq (\pi/2)^2(4j+3)\sqrt{(4j+7)(4j-1)}$ (corresponding to columns with $i > 1$ odd in Table 3).

i	1	2	3	4	5	6	7	8
ω_0	0	44.36	74.4	182.1	259.4	398.8	517.4	694.6
k_0^+	2π	8.26	9.83	14.25	16.7	20.5	23.2	26.7
$(k_0^+ \bmod 2\pi)/(\pi/2)$		1.26	2.26	1.07	2.65	1.03	2.76	1.02
k_0^-	0	5.37	7.56	12.8	15.5	19.5	22.3	25.98

Table 3: First height solutions of $P_3(\omega_0) = 0$ (see Eq. (37)).

6. Discussion and Conclusion

We have studied the vibrations of a slender planar elastic Timoshenko beam around its post-buckled equilibrium configuration, in the rigid loading case. We have shown that after buckling there is a narrow window in the loading parameter values in which half of the vibration frequencies vary abruptly. The equilibrium and dynamics of a slender elastic beam is mainly driven by flexural deformations except in this narrow window where the beam behavior is mainly extensional. The existence of these jumps for other boundary conditions such as in the dead loading case, or in the pinned-pinned case remain to be studied.

In the elastica case, the abrupt change in the frequencies becomes a discontinuous jump. This jump viewed from a theoretical point of view is rather surprising and unexpected. Indeed, Equations (13) can be easily recast in the form of a classical eigenvalue problem

$$\mathcal{L}\mathbf{X} = \omega^2 \mathcal{M}\mathbf{X} \tag{40}$$

where $\mathbf{X}$ is the six-dimensional vector build from the six normal mode variables, $\mathcal{L}$ is a first order linear linear operator in $L^2([0,1])$, (the set of square integrable functions on the unit interval)

and $\mathcal{M}$ is an inertia matrix. Therefore, a naive application of the classical theory of perturbation of eigenvalues for linear operators would suggest that once the eigenvalues have been found for a value of the control parameter, they can be locally continued in this parameter. That is we would expect the existence of a locally continuous curve for the frequencies as a function of the load close to the critical value at buckling. While it is true for some frequencies, other frequencies disappear while yet other frequencies emerge. The fundamental mathematical reason for this phenomena is that both the null spaces of the inertia matrix $\mathcal{M}$ and the linear operator $\mathcal{L}$ have a non-empty intersection in the elastica case. Mathematically, the classical theory does not apply and new conditions for the analytic continuation of frequencies with respect to the parameters emerge. Some frequencies satisfy these relations (and hence can be analytically continued) while others cease to exist. Finally, also due to the joint degeneracy of $\mathcal{M}$ and $\mathcal{L}$, there exists a continuous family of solution at the critical load given by an arbitrary increase along $\bar{n}_x$. For larger values of the load, some of these new solutions are selected and emerge, apparently out of the blue. The mathematical structure of these linear problems and how they are related to various limits (nearly inextensible rods) deserves further attention.

We now further discuss the first mode. This mode emerges from $\omega = 0$ at buckling, in the Timoshenko beam case. In Fig. 9-(a), we plot ω as function of the rise of the arch at its mid-point: $y_e(1/2) = Y_e(L/2)/L$. Each curve corresponds to a different value of the parameter η, from

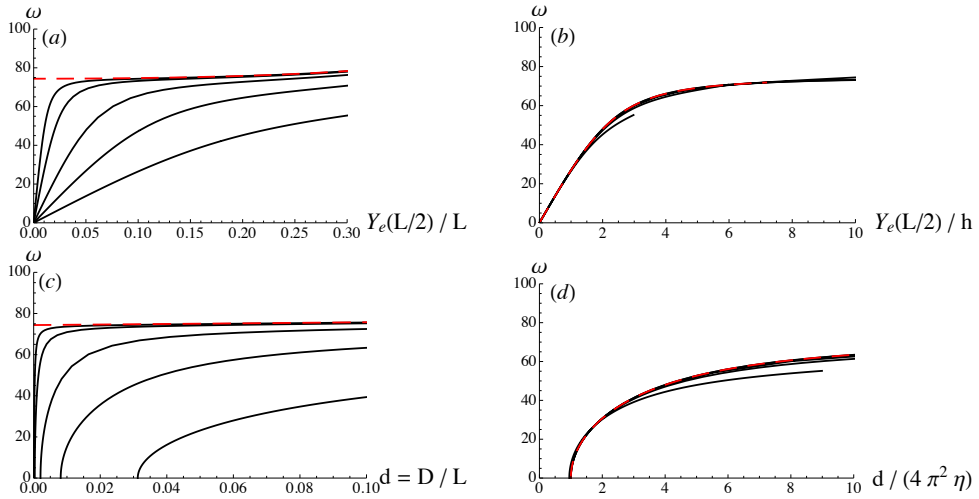

Figure 9: Post-buckled frequency of the mode emerging from $\omega = 0$ at buckling. (a) Continuous curves are for $1/\eta = 1200, 4800, 19200, 120000, 480000$ and dashed curve is for $\eta = 0$. (b) Same data but with horizontal axis rescaled with h: continuous curves for $\eta > 0$ collapse on a master curve whose slope at the origin is $\simeq 28$, and dashed curve is the first mode solution of (42) whose slope at the origin is $2\sqrt{2}\pi^2 \simeq 27.9$. (c) Same data but with $d = D/L$ on the horizontal axis. (d) Same data, collapsed once the horizontal axis is rescaled by a factor $1/(4\pi^2\eta)$, together with the dashed curve which is the first mode solution of (42).

$\eta = 1/1200$ (i.e. $L = 10\,h$) to $\eta = 1/480\,000$ (i.e. $L = 200\,h$). We see that all curves emerge from $\omega = 0$ at buckling ($y_e(1/2) = 0$) and asymptotically tend to the curve computed in the elastica case, when $y_e(1/2)$ becomes large. For very small η values, curves rise sharply from $\omega = 0$ and quickly approaches the elastica asymptote. As a matter of fact these curves can be made to almost collapse on a master curve if the horizontal axis is plotted in unit of the beam thickness h: in Fig. 9-(b) we plot the pulsation ω as function of $Y_e(L/2)/h$, for the same set of η values. All

curves nearly collapse on a master curve which has a (numerically determined) slope $\simeq 28$ at the origin. In dimensional form (i.e. $\Omega = \omega \sqrt{EI/(\rho hb)}\,/L^2$) we have then the following expression for the pulsation Ω (in rad/s):

$$\Omega \simeq 8.1\, \frac{Y_e(L/2)}{L^2} \sqrt{\frac{E}{\rho}}\,, \quad \text{for } Y_e(L/2) \lesssim 2h. \tag{41}$$

This expression shows that directly after buckling and for a short loading interval (i.e. $Y_e(L/2) = 0$ to $Y_e(L/2) \simeq 2h$), the lowest mode of vibration of a buckled beam is of extension-compression type. We also see in Fig. 9-(b) that for $Y_e(L/2) \gtrsim 6h$ the behavior is of flexural type. This separation between two different behaviors in the elastic response of the arch could be a new way to define the notion of a shallow arch: a shallow (resp. deep) arch has a vibrational response that is primarily extensional (resp. flexural).

We remark that an alternative equation is used in (for example) [8, 9, 10, 11] for the vibrations of the post-buckled arch. The transverse displacement $Y(S,T)$ is there solution of the equation:

$$EI\, Y'''' + \rho\, h\, b\, \ddot{Y} + PY'' = 0 \tag{42a}$$

$$\text{with } P = \frac{Ehb}{L}\left(D - \frac{1}{2}\int_0^L Y'^2 dS\right) \tag{42b}$$

In this model, where a certain number of assumptions on the nonlinear terms have been made, the pulsation of the first mode just after buckling is calculated to be:

$$\Omega = \sqrt{2/3}\,\pi^2\, \frac{Y_e(L/2)}{L^2} \sqrt{\frac{E}{\rho}} \tag{43}$$

where $\sqrt{2/3}\,\pi^2 \simeq 8.06$, in agreement with our prediction (41). We also show in Fig. 9-(b) and (d) the first mode solution of Eq. (42) further away from buckling, and we note this solution is independent of η, which is not rigorously the case for Kirchhoff equations. A more comprehensive comparison of the two models is the subject of a forthcoming paper.

An interesting situation arises when the first mode intersects with the second mode. This can be easily obtained by computing an approximation of the arch rise $Y_e(L/2)$ for which the first mode pulsation $\omega^{(1)} \simeq 28\, Y_e(L/2)/h$ meets the second mode pulsation $\omega^{(2)} \simeq 44.36$. This happens for $Y_e(L/2) \simeq 1.6h$. At this heigh the shape of the fundamental mode changes from a single bump wave to a double bump wave. Returning to our original motivation, we note that piano soundboards are precisely tuned in this parameter range (e.g. $h = 1$ cm, $L = 2$ m, and $Y_e(L/2) = 1$ cm). To which extent this toy model is relevant for the real problem of the piano soundboard and whether piano manufacturers are using the distinction between shallow and deep arches to enrich the sound is a tantalizing idea that deserves further attention.

Acknowledgements

It is a pleasure to thank Olivier Thomas for discussions on Eq. (42). This publication is based in part upon work supported by Award No. KUK-C1-013-04, made by King Abdullah University of Science and Technology (KAUST) (AG). AG is a Wolfson/Royal Society Merit Award holder.

References

[1] L. Virgin, Vibration of axially loaded structures, Cambridge University Press, 2007.

[2] C. Touzé, O. Thomas, A. Chaigne, Hardening/softening behaviour in non-linear oscillations of structural systems using non-linear normal modes, Journal of Sound and Vibration 273 (2004) 77 – 101.

[3] P. H. Bilhuber, C. A. Johnson, The influence of the soundboard on piano tone quality, The Journal of the Acoustical Society of America 11 (1940) 311–320.

[4] A. Mamou-Mani, J. Frelat, C. Besnainou, Numerical simulation of a piano soundboard under downbearing, The Journal of the Acoustical Society of America 123 (2008) 2401–2406.

[5] A. Mamou-Mani, J. Frelat, C. Besnainou, Prestressed soundboards: Analytical approach using simple systems including geometric nonlinearity, Acta Acustica united with Acustica 95 (2009) 915–928.

[6] A. Chaigne, C. Touzé, O. Thomas, Nonlinear vibrations and chaos in gongs and cymbals, Acoustical Science and Technology 26 (2005) 403–409.

[7] S. S. Antman, Nonlinear problems of elasticity, Springer-Verlag, New York, 2nd edition, 2004.

[8] S. Woinowsky-Krieger, The effect of an axial force on the vibration of hinged bars, ASME J. Appl. Mech. 17 (1950) 35–36.

[9] N. Yamaki, A. Mori, Non-linear vibrations of a clamped beam with initial deflection and initial axial displacement, part i: Theory, Journal of Sound and Vibration 71 (1980) 333 – 346.

[10] N. Yamaki, K. Otomo, A. Mori, Non-linear vibrations of a clamped beam with initial deflection and initial axial displacement, part ii: Experiment, Journal of Sound and Vibration 71 (1980) 347 – 360.

[11] A. Nayfeh, S. Emam, Exact solution and stability of postbuckling configurations of beams, Nonlinear Dynamics 54 (2008) 395–408.

[12] L. Euler, Methodus inveniendi lineas curvas maximi minimivi propreitate gaudentes, Opera Omnia I 24 (1744) 231–297.

[13] V. G. A. Goss, The history of the planar elastica: Insights into mechanics and scientific method, Science & Education 18 (2009) 1057–1082.

[14] M. Nizette, A. Goriely, Toward a classification of Euler-Kirchhoff filaments, J. Math. Phys 40 (1999) 2830–2866.

Appendix A. Closed form solution for the planar elastica

In the inextensible, unshearable case, the solution of system (10) with $\ddot{x}_e = 0$ and $\ddot{y}_e = 0$ corresponds to the equilibrium of the planar elastica, first studied by Euler [12] (see [13] for a historical account).

Closed form solutions of these equations can be written in term of elliptic functions, see e.g. [14]. In particular the continuous line in Fig. 2 has the parametrical expression:

$$p = 16\,K(\lambda)^2 \tag{A.1}$$

$$d = 2\left(1 - \frac{E(\lambda)}{K(\lambda)}\right)^2 \tag{A.2}$$

with $\lambda \in [0, 1)$. The elliptic integrals are defined as $K(\lambda) = \int_0^{\pi/2} \left(1 - \lambda \sin^2\theta\right)^{-1/2} d\theta$ and $E(\lambda) = \int_0^{\pi/2} \left(1 - \lambda \sin^2\theta\right)^{1/2} d\theta$. Developing Eqs. (A.1) and (A.2) for $\lambda \ll 1$ yields Eqs. (22d) and (23) with $\epsilon^2 = 4\lambda$.

Appendix B. Kinematics in 'Strength of materials' notations

In section 2, we have introduced the Cosserat-Kirchhoff notations where the normal force N_1 is related to the extension e_1 through the constitutive law (6) and where the current position (X, Y) of the central axis of the beam is given by Eqs. (8a) and (8b); all these quantities being

functions of the arc-length S of the reference configuration $(X_{\rm ref}, Y_{\rm ref}) = (S, 0)$. In 'Strength of materials' notations one uses the displacements (see Fig.1):

$$U = X - S\,, \quad V = Y, \tag{B.1}$$

also functions of the arc-length S of the reference configuration. In the current configuration the derivative of the current position with regard to S will not yield a unit vector if extension occurs. If we restrict to the case where shear in not present (i.e. $e_2 = 0$), we have $X'(S)^2 + Y'(S)^2 = (1 + e_1)^2$ which yields:

$$U' + \frac{1}{2}V'^2 - e_1 = \frac{1}{2}(e_1^2 - U'^2)\,. \tag{B.2}$$

Usually the right-hand side is neglected and the following approximation is used:

$$U' + \frac{1}{2}V'^2 - e_1 \simeq 0. \tag{B.3}$$

Appendix C. Analytical formulas for the roots of the functions P_1, P_2, and P_3

In the limit of large k_0^+, that is in the limit of large $k_0^- = \sqrt{k_0^{+2} - 4\pi^2}$ and high pulsations $\omega_0 = k_0^+ k_0^-$, we have:

$$k_0^- \simeq k_0^+ - \frac{2\pi^2}{k_0^+} - \frac{2\pi^4}{k_0^{+3}} + O\left(\frac{1}{k_0^{+5}}\right). \tag{C.1}$$

Function $P_1(\omega_0)$ (see Eq. (29)) then reads:

$$P_1(\omega_0) \simeq e^{k_0^-}\left[k_0^{+2}\cos k_0^+ + 2\pi^2\left(\sin k_0^+ - \cos k_0^+\right)\right], \tag{C.2}$$

and the solutions to $P_1(\omega_0) = 0$, for large k_0^+, are:

$$k_0^+ \simeq \frac{\pi}{2} + \frac{1}{2j^2} + 2j\pi \quad \text{with } i = 2j \tag{C.3}$$

$$k_0^+ \simeq \frac{3\pi}{2} + \frac{1}{2j^2} + 2j\pi \quad \text{with } i = 2j + 1 \tag{C.4}$$

where j is a large integer, and i is the mode number (i.e. column number in Table 1). In the same limit of high pulsations, function $P_2(\omega_0)$ (see Eq. (32)) reads:

$$P_2(\omega_0) \simeq \frac{1}{2}\, e^{k_0^-}\left[k_0^{+4}\left(\sin k_0^+ - 1\right) + 2\pi^2 k_0^{+2}\cos k_0^+ + 6\pi^4\right], \tag{C.5}$$

and the solutions to $P_2(\omega_0) = 0$, for large k_0^+, are:

$$k_0^+ \simeq \frac{\pi}{2} - \frac{3}{2j^2} + 2j\pi \quad \text{with } i = 2j - 1 \tag{C.6}$$

$$k_0^+ \simeq \frac{\pi}{2} + \frac{1}{2j^2} + 2j\pi \quad \text{with } i = 2j \tag{C.7}$$

where j is a large integer, and i is the mode number (i.e. column number in Table 2). In the same limit of high pulsations, function $P_3(\omega_0)$ (see Eq. (37)) reads:

$$P_3(\omega_0) \simeq e^{k_0^-}\left[4k_0^{+3}\left(1 - \sin k_0^+\right) + k_0^{+4}\cos k_0^+ + 2\pi^2 k_0^{+2}\right], \tag{C.8}$$

and the solutions to $P_3(\omega_0) = 0$, for large k_0^+, are:

$$k_0^+ \simeq \frac{\pi}{2} + \frac{1}{2j^2} + 2j\pi \quad \text{with } i = 2j \tag{C.9}$$

$$k_0^+ \simeq \frac{3\pi}{2} - \frac{4}{\pi j} + 2j\pi \quad \text{with } i = 2j + 1 \tag{C.10}$$

where j is a large integer, and i is the mode number (i.e. column number in Table 3). We see that in this limit the three functions P_1, P_2, and P_3 share half of their roots, namely those given by (C.3), (C.7), or (C.9).

RECENT REPORTS

14/11	A Constrained Approach to Multiscale Stochastic Simulation of Chemically Reacting Systems	Cotter Zygalakis Kevrekidis Erban
15/11	The Two Regime Method for optimizing stochastic reaction-diffusion simulations	Flegg Chapman Erban
16/11	Recombination via tail states in polythiophene:fullerene solar cells	Kirchartz Pieters Kirkpatrick Rau Nelson
17/11	Energy versus electron transfer in organic solar cells: a comparison of the photophysics of two indenofluorene: fullerene blend films	Soon Clarke Zhang Agostinelli Kirkpatrick Dyer-Smith McCulloch Nelson Durrant
18/11	Asymptotic analysis of a pile-up of edge dislocation	Hall
19/11	A perturbation analysis of spontaneous action potential initiation by stochastic ion channels	Keener1 Newby
20/11	Hybrid modelling of individual movement and collective behaviour	Franz Erban
21/11	A novel model for one-dimensional morphoelasticity. Part I: Theoretical foundations	Hall Menon McCue McElwain
22/11	A novel model for one-dimensional morphoelasticity. Part II: Application to the contraction of fibroblast-populated collagen lattices	Hall Menon McCue McElwain
23/11	Positive or negative Poynting efect? The role of adscititious inequalities in hyperelastic materials	Mihai Goriely McCue McElwain
24/11	On approaches to modelling lattice dislocations	Hall Markenscoff
25/11	Nonlinear waves in heterogeneous elastic rods via homogenization	de Luna Emptage Goriely Bressloff
26/11	Synaptic bistability due to nucleation and evaporation of receptor clusters	Burlakov Duričković Goriely

29/11	Floating carpets and the delamination of elastic sheets	Wagner Vella
30/11	Numerical Study of Liquid Crystal Elastomers by a Mixed Finite	Luo Calderer
31/11	The indentation of pressurized elastic shells: From polymeric capsules to yeast cells	Vella Ajdari Vaziri Boudaoud
32/11	Wrinkling of pressurized elastic shells	Vella Ajdari Vaziri Boudaoud
33/11	Data assimilation using bayesian filters and B-spline geological models	Duan Farmer Hoteit Lu Moroz
34/11	Review of nonlinear Kalman, ensemble and particle filtering with application to the reservoir history matching problem	Luo Hoteit Duan Wang
35/11	Modelling a Tethered Mammalian Sperm Cell undergoing Hyperactivation	Curtis Kirkman-Brown Connolly Gaffney
36/11	A simple mathematical model for investigating the effect of cluster roots on plant nutrient uptake	Zygalakis Roose

Copies of these, and any other OCCAM reports can be obtained from:

Oxford Centre for Collaborative Applied Mathematics
Mathematical Institute
24 - 29 St Giles'
Oxford
OX1 3LB
England
www.maths.ox.ac.uk/occam